Electrocatalysis (2024) 15:20–28
https://doi.org/10.1007/s12678-023-00850-x

RESEARCH

Fabrication of MoS_2 with Dual Defects of O-Doping and S-Vacancies for High-Efficiency Hydrogen Production

Hongyu Zhao[1] · Hao Zhang[1] · Ruoyu Huang[1] · Jianmin Wang[1] · Jiajia Cai[1] · Jing Hu[1] · Zhijie Chen[1] · Yongtao Li[1] · Haijin Li[1]

Accepted: 23 October 2023 / Published online: 2 November 2023

Abstract

Developing excellent electrocatalysts is a significant step in accelerating the widespread implementation of the electrochemical hydrogen evolution reaction (HER). MoS_2 is one of the promising alternatives to platinum-based catalysts, while its HER activity is far from Pt due to the lack of active sites. It is urgent to develop a novel strategy to activate the basal planes of MoS_2 for enhancing the HER activity. Herein, a facile hydrothermal method with a low-temperature H_2O_2 etching method is developed to fabricate MoS_2 with O-doped and S-vacancy dual defects. The dual defects MoS_2 nanosheet demonstrates remarkable hydrogen evolution reaction (HER) activity, achieving 10 mA cm^{-2} with a small overpotential of around 143 mV in 0.5 M H_2SO_4.

Keywords Molybdenum disulfide · O-doping · S-vacancies · H_2O_2 etching

Introduction

Developing clean hydrogen is significant to achieving the target of carbon neutrality. Electrocatalytic hydrogen evolution has garnered significant interest due to its potential to be fueled by green energy sources [1, 2]. However, practical implementation of the method is currently hindered by the lack of affordable, efficient, and stable catalysts [3–5]. So, it is imperative to manufacture highly active non-noble metal electrodes through material innovation. Electrocatalysts that are abundant on Earth, such as transition metal alloys [6, 7], chalcogenides, nitrides [8], and phosphides [9], are thoroughly studied and intensively developed for HER. Among them, a lot of attention has been put into 2D transition metal dichalcogenide (2D TMD), especially to molybdenum disulfide (MoS_2), which exhibits optimized hydrogen adsorption energy (ΔG_{H^*}). Limited active sites still restrict the HER activity of MoS_2-based electrocatalysts, despite considerable work being dedicated to this field.

In-depth studies demonstrate that only the edge sites and coordinate unsaturated atoms are active areas. However, the catalytic capacity of basal planes is poor [10–12]. Therefore, increasing the active site density of electrocatalysts is a unique way to strengthen the MoS_2 HER performance, which includes maximizing exposure of edge sites and activating basal planes. Recently, a lot of studies have been committed to expose more edge sites such as nanostructure engineering [13–16], and phase engineering [17–20]. However, due to the basal planes constituting the majority of the bulk material, making use of them is essential to the development of MoS_2. Heteroatom doping has been considered to be an excellent route to expose the basal plane owing to dopants with varying electronegative properties that will change the electronic structure of MoS_2 [13, 16, 17]. Among these dopants, O-doping has been proved not only to provide abundant unsaturated sulfur atom sites for active sites [18] but also to improve the conductivity, thus boosting the HER activity of MoS_2 [19]. However, how to prepare MoS_2 with controlled O contents is still a huge challenge. Furthermore, modulating S-vacancies into MoS_2 has been recognized as an effective method for active inert basal planes [12, 21–27]. Many efforts have been made to introduce S-vacancies into the basal planes, such as plasma

✉ Jianmin Wang
wjmahut@ahut.edu.cn

✉ Haijin Li
lihaijin@ahut.edu.cn

[1] School of Energy and Environment, Anhui University of Technology, Ma'anshan, Anhui 243002, People's Republic of China

etching [24], H_2 reduction [25], and electrochemical reduction [23, 26]. These approaches are tool-dependent, expensive, or operationally dangerous. More recently, wet chemical etching such as NaClO [27], NH_4F [18], and H_2O_2 [22] etching has been developed for the formation of S-vacancies. In particular, a mild H_2O_2 etching method is used to introduce evenly distributed S-vacancies into MoS_2, which exhibits outstanding HER activity. However, because of the strong binding energy of Mo-S, controlling the rate of S-vacancy formation remains a challenge. It is well known that the S^{2-} in defective-rich MoS_2 is easier to leach compared to complete MoS_2. Therefore, it is reasonable to deduce that the MoS_2 with O doped is easier to generate S-vacancies via H_2O_2 etching and will also present outstanding HER activity.

Herein, we demonstrate a novel strategy to construct dual-defect MoS_2 via a facile hydrothermal method and mild H_2O_2 etching process. The results show that O-doping not only increases the density of active sites but also facilitates the addition of S-vacancies. Owing to the combined contribution of O-doping and S-vacancies, a distinct enhancement of the dual-defect MoS_2 is achieved compared to pristine MoS_2, as well as high stability in an acid medium. The study may offer a promising way to realize the potential of inert basal planes of MoS_2 electrocatalysts to achieve high HER activity.

Experimental Section

Chemicals and Materials

Analytical-grade reagents including ammonium molybdate tetrahydrate ($(NH_4)_6Mo_7O_{24}{\cdot}4H_2O$), thiourea, KOH, and H_2O_2 (≈ 30 wt %) were procured from Aladdin Industrial Corporation and Shushi, respectively. The carbon paper (CP) used in the experiment, with a thickness of 0.21 mm, was supplied by HESEN Company. No further purification of these reagents was deemed necessary for the study.

Preparation of MoS_2 O-MoS_2 and O-MoS_2-x

To synthesize oxygen-doped MoS_2 nanosheets on carbon paper, a one-step hydrothermal method was employed. Briefly, a uniform solution was prepared by mixing 7 mM $(NH_4)_6Mo_7O_{24}{\cdot}4H_2O$ and 250 mM thiourea in 20 mL of deionized water. The solution was then transferred into a Teflon-lined autoclave along with a cleaned CP substrate (1 cm × 2 cm) for MoS_2 growth, which was heated at 200 °C for 18 h. Following this, the resulting product, named O-MoS_2, was washed with water under sonication and dried in a vacuum oven at 60 °C for 12 h.

To introduce S-vacancies and O-doping in the O-MoS_2 nanosheets, a chemical etching method was applied. In this process, the as-prepared O-MoS_2/CP was immersed in an H_2O_2 solution with a concentration of 3 M at 0 °C for 20 s, followed by rinsing in deionized water. The resulting sample was denoted as O-MoS_2-x. For comparative purposes, samples treated with different concentrations of H_2O_2 (1 M, 3 M, 5 M, 10 M) under identical conditions were prepared and named O-MoS_{2-x}-1, O-MoS_{2-x}-2, O-MoS_{2-x}-3, and O-MoS_{2-x}-4. Additionally, a sample without O-doping and S-vacancies was synthesized using thermal treatment at 350 °C under a sulfur atmosphere for 2 h, referred to as MoS_2.

Characterization

To characterize the obtained samples, X-ray diffraction (XRD) tests were performed on an Ultima (Japan) powder diffraction system at a scan rate of 5° min^{-1}. The morphologies of the samples were examined using a field-emission scanning electron microscope (FE-SEM) NANO SEM430, while Raman spectroscopies were conducted using a Renishaw inVia. Furthermore, high-resolution transmission electron microscopy (HRTEM) images were obtained using a JEM-2100. The XPS survey spectrum was measured on Thermo Fisher Scientific ESCALAB Xi+.

Electrochemical Measurements

All electrochemical experiments were conducted using an electrochemical workstation (CHI760E) and a standard three-electrode system, with O-MoS_{2-x} serving as the working electrode, platinum plate as the counter electrode, and silver chloride electrode as the reference electrode. All potentials were calibrated to a reversible hydrogen electrode (RHE). For the linear sweep voltammetry (LSV) measurements used to evaluate overall water splitting, a scan rate of 5 mV s^{-1} was employed. Long-term potential cycling was assessed through continuous cyclic voltammetry (CV) at a scanning rate of 50 mV s^{-1} for 1000 cycles, within a potential range of −0.2 to −0.5 V (vs RHE). The C_{dl} values of the electrodes in the double-layer region (excluding Faraday processes) were calculated using CV at different scanning rates (10–50 mV s^{-1}). Furthermore, Nyquist plots were obtained at a potential of −0.1 V (vs RHE) over a frequency range of 100 kHz to 0.1 Hz for impedance analyses.

Results and Discussion

Scheme 1 illustrates the procedure for forming MoS_2 with oxygen-doping and S-vacancies. Firstly, oxygen-doped MoS_2 nanosheets were synthesized on the surface of CP through a relatively low-temperature hydrothermal method.

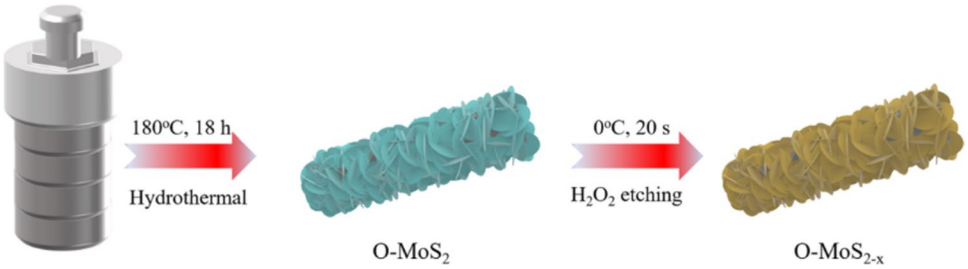

Scheme 1 Schematic representation of the preparation of O-MoS_{2-x}

Subsequently, the obtained O-MoS_2/CP was immersed in H_2O_2 for 20 s. The reaction between S^{2-} and H_2O_2 leads to the successful generation of S-vacancies.

The FE-SEM was used to discuss the microscopic morphology of O-MoS_2/CP and O-MoS_2-x/CP (Fig. 1a, b). The upright orientation and homogeneous dispersion of O-MoS_2/CP on the carbon fiber surface are visible; such a hierarchical structure provides a larger reaction area. Meanwhile, the increase of catalyst reaction area can often alleviate the hysteresis of electrolyte conduction caused by confining in mesoporous, which accelerates the HER reaction between the O-MoS_{2-x} surface and electrolyte [28, 29]. The magnified SEM image reveals that the nanosheets are about 22 nm in thickness, which exposes a larger portion of the catalytically active sites, and thus conducive to a higher rate of charge transfer [30]. For the obtained O-MoS_{2-x}/CP, the density of the nanosheets is slightly reduced compared to pristine samples, as shown in the inset Fig. 1b, which is demonstrated more vividly in the locally magnified image in Fig. 1b. Furthermore, the SEM image indicates a slight decrease in the average thickness of MoS_2. It shows that the morphology of MoS_2 remains unchanged after the reaction with H_2O_2, indicating that the etching occurs only on the surface of the nanosheets. The microstructure changes after H_2O_2 etching are further investigated by TEM. The nanosheets of O-MoS_{2-x}/CP were peeled off from the CP by the sonication method. As shown in Fig. 1c, noticeable lines and ripples can be noted, suggesting the ultra-thinness of the samples, which is in line with the findings (Fig. S1) for the original O-MoS_2/CP. Enlarged TEM and HRTEM images show that the vertical nanosheets have only 10–15 layers of MoS_2, providing a shorter charge transfer path and exposing a greater fraction of the catalytically active sites, which enhances the reaction kinetics [31, 32]. As shown in Fig. 1d, the spacing of interlayer distance is 0.64 nm for O-MoS_{2-x}/CP, which corresponds to the (002) phase of MoS_2. Notably, the distance for O-MoS_{2-x}/CP is smaller than that of 0.67 nm for O-MoS_2/CP (Fig. 1e), mainly owing to the formation of S-vacancies. The decrease in interlayer distance, driven by S-vacancies, can be attributed to the significant reconstruction of Mo atoms within the MoS_2 bilayer. Specifically, the undercoordinated Mo atoms tend to form bonds with the nearest S atom, resulting in the lattice contraction [33, 34].

Interestingly, the interlayer distance is larger than the MoS_2 as reported before, which could contribute to the incorporation of O, and the expanded interlayer distance is favorable for catalytic performance. Meanwhile, the STEM images and corresponding EDS mappings indicate that Mo, S, and O are uniformly distributed throughout the MoS_2 nanosheet, which suggests successful and uniform O-doping in MoS_2.

The X-ray diffraction (XRD) was initially used to confirm the crystal structures of O-MoS_2/CP and O-MoS_2-x/CP (Fig. 2a). The diffraction peaks at 13.9, 33.4, and 59.1°, respectively, align with the (002), (100), and (110) planes of MoS_2 (PDF#75–1539). Specifically, the significant peak in the low-angle area (17.8°) is also observed, which is due to the lattice expansion caused by the doping of O. Furthermore, it can be seen from the XRD pattern that the slight H_2O_2 etching does not cause the crystal phase change of O-MoS_2.

Additionally, Raman spectroscopy was used to analyze the structures of MoS_2 and O-MoS_2-x (Fig. 2b). Notably, the E_{2g} and A_{1g} modes of Mo-S bonds give rise to the main peaks at 378 and 409 cm^{-1}, respectively. Furthermore, the presence of the B_{2g} and B_{1g} vibrational modes in the Raman spectra, recorded at 282 and 336 cm^{-1}, indicates the formation of Mo–O bonds and O-Mo_3, respectively, demonstrating the existence of O in the as-prepared samples. The decrease in the characteristic peak of MoS_2 and increase in Mo–O bonds observed upon comparing the patterns of MoS_2 and O-MoS_2-x indicate that the doping of O not only increases the density of active sites but also promotes the addition of S-vacancies. After H_2O_2 etching, the peaks of Mo–O (282 cm^{-1}) and OMo_3 (336 cm^{-1}) were further enhanced, while the peaks of Mo-S (378 and 404 cm^{-1}) were weakened, indicating that H_2O_2 etching increases the content of O element and S-vacancies of O-MoS_2. These results support the conclusion that O-MoS_{2-x} has been synthesized with the inclusion of O-doping and S-vacancies.

To determine the elemental composition and bonding configuration in the synthesized sample, the XPS survey spectrum (Fig. 3) was taken on the O-MoS_2 and O-MoS_{2-x} nanosheets to study the chemical states of the elements on the surface of the samples. Figure 3a is the total XPS spectrum, from which it can be seen that the content of O

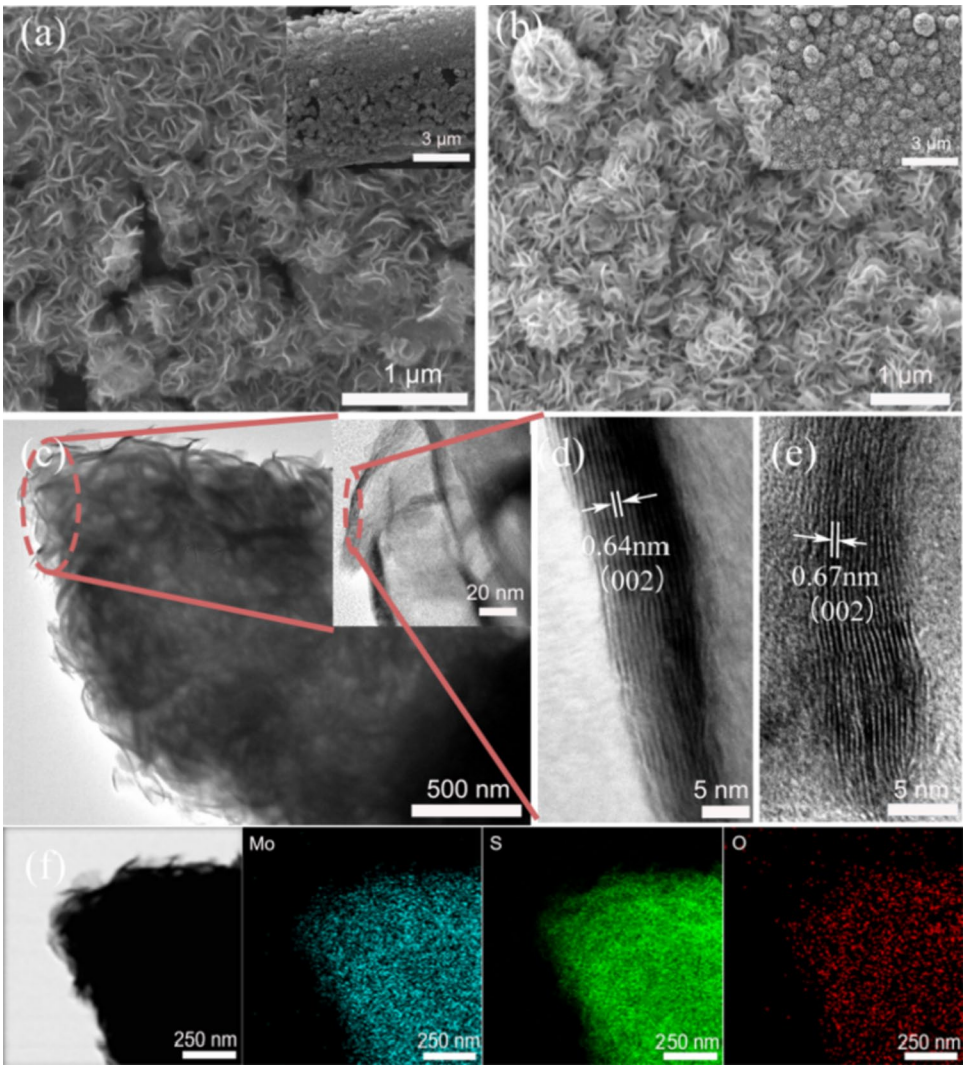

Fig. 1 Structural, morphology, and elemental analysis of O-MoS_2/CP and O-MoS_{2-x}/CP. SEM for **a** O-MoS_2/CP and **b** O-MoS_{2-x}/CP. The insets show the low-resolution SEM images of the samples. **c** TEM and **d** HRTEM image for O-MoS_{2-x}/CP. **e** HRTEM for O-MoS_2/CP. **f** EDS mapping for O-MoS_{2-x}/CP

is greatly increased after H_2O_2 etching, suggesting the success of O-doping. In the high-resolution Mo 3d XPS spectrum in Fig. 3b, two major peaks are distinctly observed at 229.3 and 232.4 eV, which can be assigned to the Mo 3d 5/2 and Mo 3d 3/2 in O-MoS_{2-x}, whereas the signal at 226.3 eV is attributed to the S 2 s electrons. The deconvolution of S 2p peaks (Fig. 2d) gives rise to 161.8 and 163.2 eV, which is attributed to S 2p3/2 and S 2p5/2. After H_2O_2 etching, the core peaks of S 2p and Mo 3d show 0.2 eV shifts towards higher binding energies, which are related to S-vacancies [35]. Additionally, the S–O peaks at 168.9 were observed in the S 2p spectra. Combined with Fig. 3a, c (O 1 s), it is proved that O-MoS_2 is successfully doped with O. The above results further demonstrate that the O-doping and S-vacancy-modified O-MOS_{2-x} are successfully obtained by H_2O_2 etching, which corresponds to the Raman spectra.

To assess the electrocatalytic properties, MoS_2 samples with different defects were subjected to LSV (0.5 M H_2SO_4). The HER performance of O-MoS_2 is greatly optimized after the incorporation of oxygen atoms and further formation of S-vacancies. O-MoS_2-x exhibits significantly lower overpotential required (10 mA cm^{-2}). Figure 4b shows the overpotential of all samples to reach different current densities. O-MoS_2-x demonstrates a much better electrocatalytic performance than O-MoS_2 and MoS_2, as evidenced by the significantly lower overpotential of approximately 143 mV required at 10 mA cm^{-2}. When reaching 50 mA cm^{-2}, the O-MoS_{2-x} requires only 202 mV, which is also lower than O-MoS_2 and MoS_2.

The Tafel slope can give more insight into the kinetic mechanism of the HER process. Generally, the process of HER can be divided into two steps. Firstly, the electrochemical adsorption of hydrogen, ($H_3O^+ + e^- \rightarrow H_{ad} + H_2O$), is named the Volmer step. Subsequently, the electrochemical hydrogen desorption step exhibits two different ways: Heyrovsky step ($H_3O^+ + H_{ad} + e^- \rightarrow H_2 + H_2O$) or Tafel step ($H_{ad} + H_{ad} \rightarrow H_2$). The Tafel slopes depicted in Fig. 4c

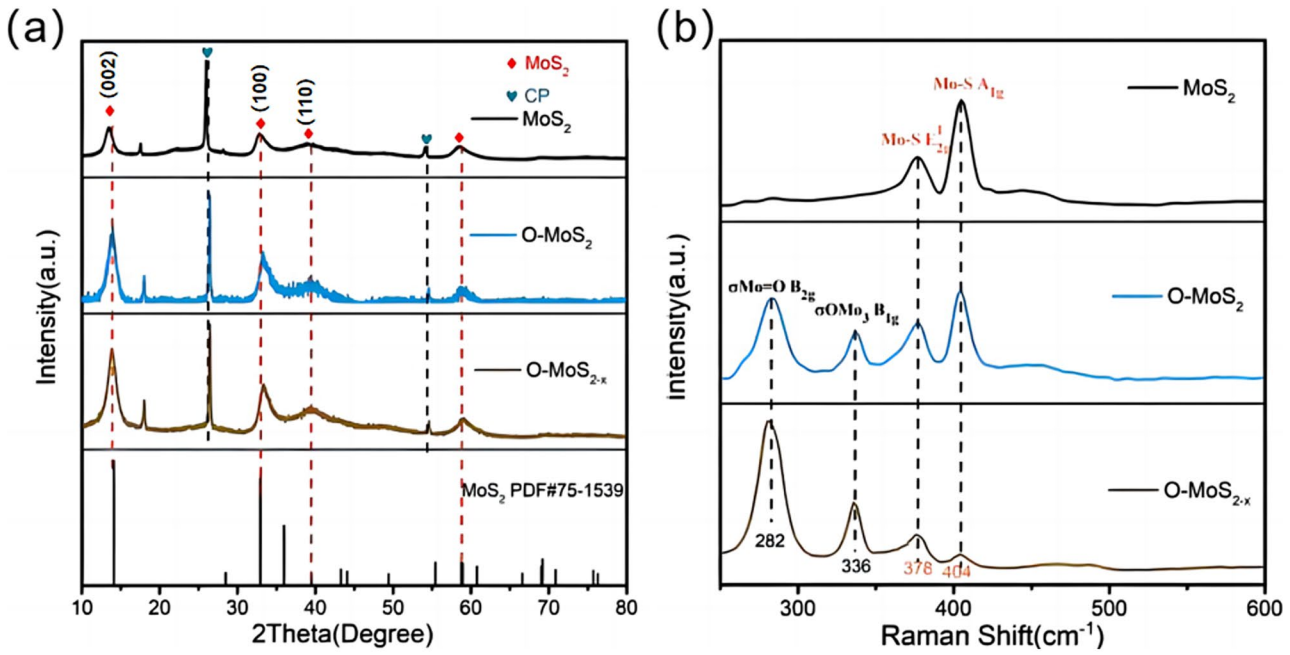

Fig. 2 **a** XRD; **b** Raman spectra of the synthesized MoS_2, O-MoS_2, and O-MoS_{2-x} electrocatalysts

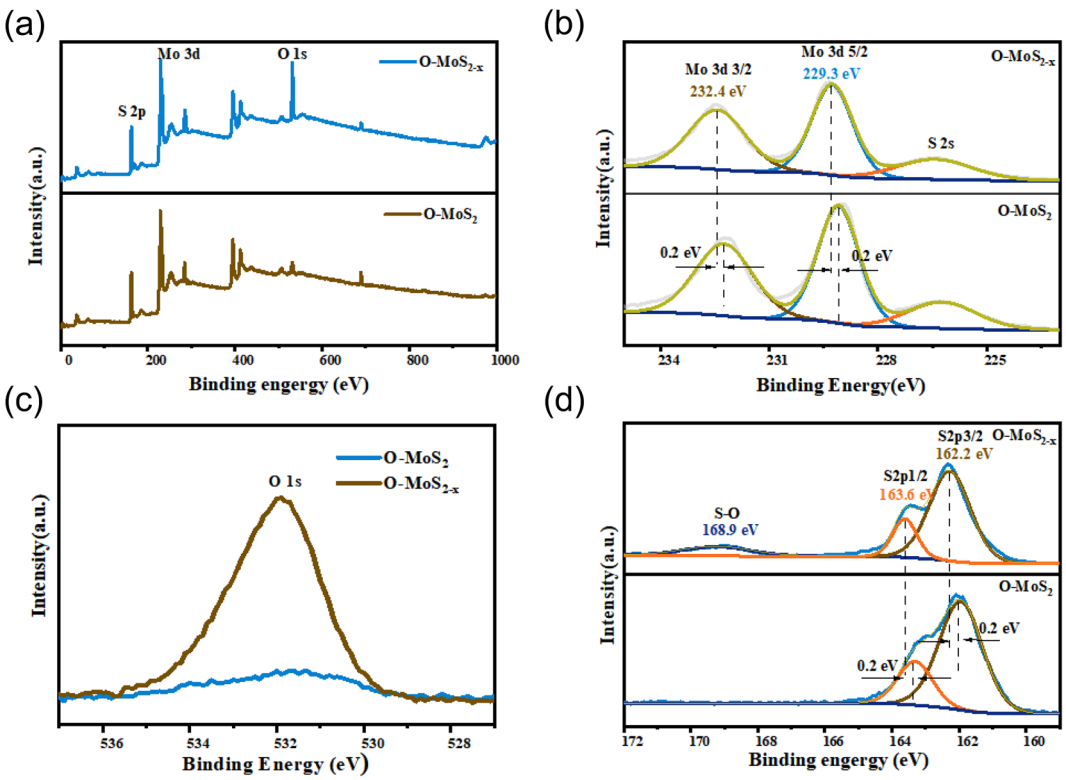

Fig. 3 XPS spectra of O-MoS_2 and O-MoS_{2-x}. **a** Survey spectra, **b** high-resolution Mo 3d XPS spectrum, **c** high-resolution O 1 s XPS spectrum, and (**d**) high-resolution S 2p XPS spectrum

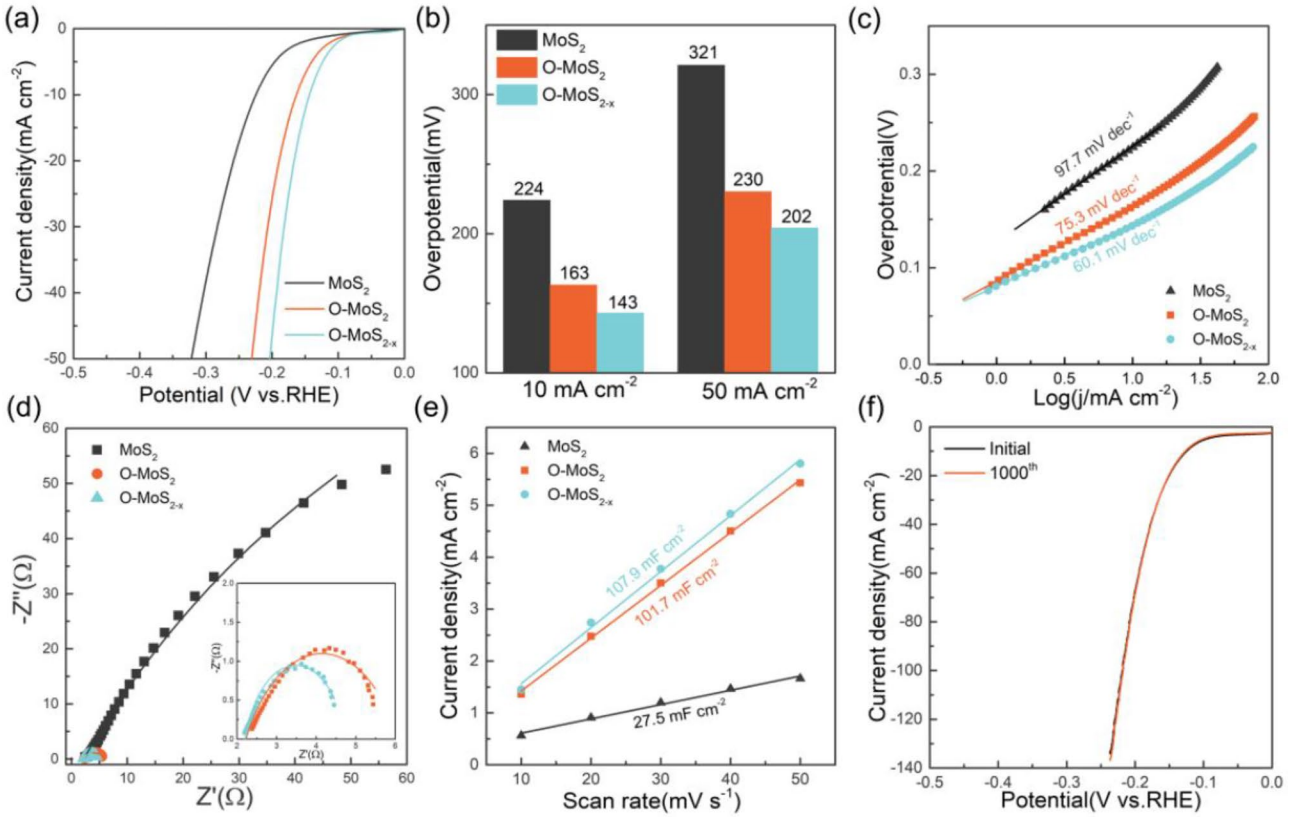

Fig. 4 **a** LSV curves of MoS_2, O-MoS_2, and O-MoS_2-x. **b** Overpotentials at 10 mA cm^{-2} and 50 mA cm^{-2}. **c** Corresponding Tafel plots. **d** Nyquist plots. **e** ECSA. **f** LSV plots after stability

are greater than 30 mV dec^{-1}, indicating that all the catalysts underwent the Volmer-Heyrovsky mechanism during the HER process. Meanwhile, the high Tafel slope recorded for pure MoS_2 at 97.7 mV dec^{-1} indicates that the rate-limiting step is the Volmer step; in other words, the hydroxonium molecule is difficult to dissociate on the MoS_2 surface. Instead, the Tafel slope decreased after the incorporation of O, which is calculated to be about 75.3 mV dec^{-1}, suggesting a shift in the rate-limiting step of the HER process on O-MoS_2, moving from the Volmer step to the Heyrovsky step. An implication of this is the possibility that the adsorption of H_3O^+ is activated through the synergy between $Mo^{\delta+}$…O and $S^{\delta-}$…H, due to the incorporation of O [19]. The formation of S-vacancies in O-MoS_2-x results in a slightly smaller Tafel slope of 60.1 mV dec^{-1}, indicating a similar HER mechanism but accelerated kinetics compared to O-MoS_2.

The HER kinetics and charge conduction properties can be studied through the utilization of Electrochemical Impedance Spectroscopy (EIS) measurements (Fig. 4d). The results clearly show that O-MoS_{2-x} enables an important reduction of resistance, promoting a faster reaction rate. The above results elucidate that the incorporation of O and the addition of S-vacancies significantly accelerate reaction kinetics.

Cyclic voltammetry (CV) is conducted within a range devoid of any faradic reaction, as illustrated in Fig. S4. The calculated C_{dl} from CV curves shown in Fig. 4e shows that the incorporation of O and S-vacancies in the sample resulted in a slight increase in the capacitance value to 107.9 mF cm^{-2}, compared to the sample lacking S-vacancies (101.7 mF cm^2), while almost 4 times higher than the pristine MoS_2 (27.5 mF cm^{-2}). It can be deduced that the doping of O into the samples facilitates the transfer of more charge, within the synergy of S-vacancies that enhances active sites even further. In conclusion, the co-promotion of incorporated O and S-vacancies can accelerate reaction kinetics and promote charge transfer, thereby significantly enhancing HER performance.

Furthermore, long-term stability is a significant parameter for O-MoS_{2-x} performance, which is evaluated by the LSV test after continuous CV cycles. Exceptionally, as shown in Fig. 4f, at a sweep rate of 50 mV s^{-1} (−0.2 ~ 0.1 V and RHE), the polarization curves exhibit a slight decrease in their values after the first and 1000th CV cycles, further stably indicating excellent stability performance. The

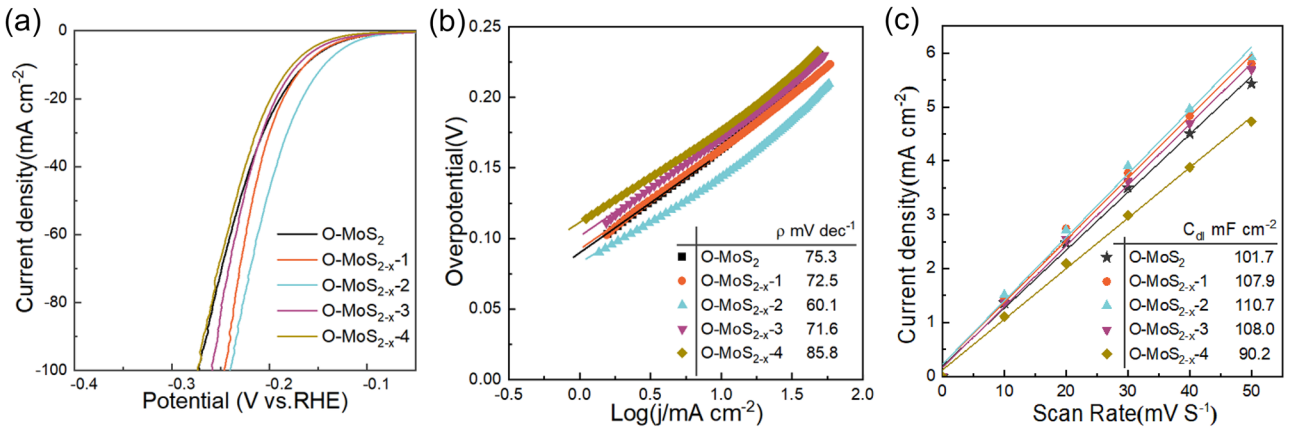

Fig. 5 The HER performance of O-MoS_2 evaluated under different densities of S-vacancies. **a** Polarization curves, **b** Tafel plots of presented data in (**a**), and **c** ECSA plots

O-MoS_2-x catalyst exhibits outstanding activity as well as remarkable stability, as revealed in the experimental findings.

To acquire a deeper comprehension of the impact of S-vacancies on the HER process, samples with varying densities of S-vacancies are prepared by modifying the concentration of H_2O_2 or the treatment time. Firstly, the samples treated with various concentrations of H_2O_2 were examined using SEM and XRD techniques (Fig. S1) to ascertain their morphology and structural characteristics. It was observed that the treated samples exhibited minimal deviation from the original O-MoS_2, thereby indirectly indicating that etching with an appropriate amount of H_2O_2 does not significantly alter the internal structure of the samples. Figure 5 illustrates the HER performance of the samples that were treated using various concentrations of H_2O_2. It can be seen that the sample treated with 3 M (O-MoS_{1-x}-2) presents the best HER activity, which exhibits a volcano trend with the increment of H_2O_2 concentration, the concentration of S-vacancies. In Fig. 5b, as expected, the sample O-MoS_{1-x}-2 exhibits the lowest Tafel slope. Within the increase of H_2O_2 concentrations, the Tafel slopes exhibit an "inverted volcanic" trend, indicating that a suitable concentration of S-vacancies effectively accelerates HER kinetics. However, excessively high S-vacancies can actually inhibit the reaction kinetically, which is probably due to the over-strong H binding caused by excessive S-vacancies. In addition to the reaction kinetics, the concentration of S-vacancies also affects the amounts of active sites. Figure 5c presents the ECSA of the samples with different concentrations of S-vacancies, which exhibits a similar trend with Tafel slopes, which indicates that the generation of S-vacancies will excite more active sites while inhibiting active sites when the S-vacancies are exceeded.

Conclusion

In conclusion, through the integration of a hydrothermal method and mild H_2O_2 etching strategy, we have successfully developed a reliable method for synthesizing dual-defects of O-doping and S-vacancy MoS_2 nanosheets on CP, which exhibit exceptional electrocatalytic performance for the HER process. The dual-defect MoS_2 nanosheets display excellent electrocatalytic activity in the HER process, as evidenced by their small overpotential of approximately 143 mV and 202 mV to reach the 10 mA cm^{-2} and 50 mA cm^{-2} in 0.5 M H_2SO_4, respectively. The increased HER performance could be attributed to the synergistic effect of O-doping and S-vacancy dual defects, which not only motivate more active sites but also accelerate the HER kinetics. This work proposes an affordable and straightforward technique for the design of high-efficiency MoS_2-based catalysts.

Supplementary Information The online version contains supplementary material available at https://doi.org/10.1007/s12678-023-00850-x.

Author Contribution Jianmin Wang: conceptualization, methodology, visualization, formal analysis, writing – original draft, investigation, data curation. Hongyu Zhao and Hao Zhang: software, visualization. Ruoyu Huang: investigation, data curation. Jiajia Cai: formal analysis.Jing Hu: formal analysis, resources. Zhijie Chen: formal analysis. Yongtao Lig: writing – review & editing, funding acquisition, supervision. Haijin Li: writing – review & editing, funding acquisition, supervision, project administration.

Funding This article received support from key projects of the Anhui Provincial Department of Education, China (Grant No. KJ2021ZD0044), the University Natural Science Research Project of Anhui Province (KJ2021A0380), and the Anhui Provincial Natural Science Foundation (1908085QE179, 2208085ME110).

Availability of Data and Materials All data that support the findings of this study are included within the article (and any supplementary files).

Declarations

Ethical Approval All procedures performed in studies involving human participants were by the ethical standards of the institutional and/or national research committee and with the 1964 Helsinki Declaration and its later amendments or comparable ethical standards.

Conflict of Interest The authors declare no competing interests**.**

References

1. O.J. Guerra, J. Eichman, J. Kurtz, B.M. Hodge, Cost competitiveness of electrolytic hydrogen. Joule. **3**, 2425–2443 (2019). https://doi.org/10.1016/j.joule.2019.07.006
2. J. Kibsgaard, I. Chorkendorff, Considerations for the scaling-up of water splitting catalysts. Nat. Energy **4**, 430–433 (2019). https://doi.org/10.1038/s41560-019-0407-1
3. J. Linnemann, K. Kanokkanchana, K. Tschulik, design strategies for electrocatalysts from an electrochemist's perspective. ACS Catal. **11**, 5318–5346 (2021). https://doi.org/10.1021/acscatal.0c04118
4. J. Song, C. Wei, Z.F. Huang, C. Liu, L. Zeng, X. Wang, Z.J. Xu, A review on fundamentals for designing oxygen evolution electrocatalysts. Chem. Soc. Rev. **49**, 2196–2214 (2020). https://doi.org/10.1039/c9cs00607a
5. S. Anantharaj, V. Aravindan, Developments and perspectives in 3D transition-metal-based electrocatalysts for neutral and near-neutral water electrolysis. Adv. Energy Mater. **10**, 1–30 (2020). https://doi.org/10.1002/aenm.201902666
6. T.F. Jaramillo, K.P. Jørgensen, J. Bonde, J.H. Nielsen, S. Horch, I. Chorkendorff, Identification of active edge sites for electrochemical H_2 evolution from MoS_2 nanocatalysts. Science **317**, 100–102 (2007). https://doi.org/10.1126/science.1141483
7. Y. Yin, J. Han, Y. Zhang, X. Zhang, P. Xu, Q. Yuan, L. Samad, X. Wang, Y. Wang, Z. Zhang, P. Zhang, X. Cao, B. Song, S. Jin, Contributions of phase, sulfur vacancies, and edges to the hydrogen evolution reaction catalytic activity of porous molybdenum disulfide nanosheets. J. Am. Chem. Soc. **138**, 7965–7972 (2016). https://doi.org/10.1021/jacs.6b03714
8. H. Li, C. Tsai, A.L. Koh, L. Cai, A.W. Contryman, A.H. Fragapane, J. Zhao, H.S. Han, H.C. Manoharan, F. Abild-pedersen, J.K. Nørskov, Activating and optimizing MoS_2 basal planes for hydrogen evolution through the formation of strained sulphur vacancies. Nat. Mater. **15**, 48–53 (2016). https://doi.org/10.1038/nmat4564
9. X. Hou, H. Zhou, M. Zhao, Y. Cai, Q. Wei, MoS_2 nanoplates embedded in Co-N-doped carbon nanocages as efficient catalyst for HER and OER. ACS Sustain. Chem. Eng. **8**, 5724–5733 (2020). https://doi.org/10.1021/acssuschemeng.0c00810
10. D. Kong, H. Wang, J.J. Cha, M. Pasta, K.J. Koski, J. Yao, Y. Cui, Synthesis of MoS_2 and $MoSe_2$ films with vertically aligned layers. Nano Lett. **13**, 1341–1347 (2013). https://doi.org/10.1021/nl400258t
11. J. Feng, Z. Zhao, R. Tang, Y. Zhao, T. Meng, Interfacial structural and electronic regulation of MoS_2 for promoting its kinetics and activity of alkaline hydrogen evolution. ACS Appl. Mater. Interfaces **13**, 53262–55327 (2021). https://doi.org/10.1021/acsami.1c17031
12. Y. Zhou, Y. Liu, W. Zhao, F. Xie, R. Xu, B. Li, X. Zhou, H. Shen, Growth of vertically aligned MoS_2 nanosheets on a Ti substrate through a self-supported bonding interface for high-performance lithium-ion batteries a general approach. J. Mater. Chem. A Mater. **4**, 5932–5941 (2016). https://doi.org/10.1039/c6ta01116k
13. J. Rong, Y. Ye, J. Cao, X. Liu, H. Fan, S. Yang, M. Wei, L. Yang, J. Yang, Y. Chen, Restructuring electronic structure via W doped 1T MoS_2 for enhancing hydrogen evolution reaction. Appl. Surf. Sci. **579**, 152216–152224 (2021). https://doi.org/10.1016/j.apsusc.2021.152216
14. X. Chen, Z. Wang, Y. Wei, X. Zhang, Q. Zhang, L. Gu, L. Zhang, N. Yang, R. Yu, High phase-purity 1T-MoS_2 ultrathin nanosheets by a spatially confined template. Angew. Chem. Int. Ed. **58**, 17621–17624 (2019). https://doi.org/10.1002/anie.201909879
15. L. Wang, X. Zhang, Y. Xu, C. Li, W. Liu, S. Yi, K. Wang, X. Sun, Z.S. Wu, Y. Ma, Tetrabutylammonium-intercalated 1T-MoS_2 nanosheets with expanded interlayer spacing vertically coupled on 2D delaminated MXene for high-performance lithium-ion capacitors. Adv. Funct. Mater. **31**, 1–11 (2021). https://doi.org/10.1002/adfm.202104286
16. R. Zhang, M. Zhang, H. Yang, G. Li, S. Xing, M. Li, Y. Xu, Q. Zhang, S. Hu, H. Liao, Y. Cao, Creating fluorine-doped MoS_2 edge electrodes with enhanced hydrogen evolution activity, Small. Methods **5**, 1–7 (2021). https://doi.org/10.1002/smtd.202100612
17. Y. Shi, Y. Zhou, D.R. Yang, W.X. Xu, C. Wang, F. Bin Wang, J.J. Xu, X.H. Xia, H.Y. Chen, Energy level engineering of MoS_2 by transition-metal doping for accelerating hydrogen evolution reaction, J. Am. Chem. Soc. **139**, 15479–15485 (2017).https://doi.org/10.1021/jacs.7b08881
18. X. Yang, X. Li, Y. Wang, C. Ye, Z. Du, H. Yu, J. Liu, L. Chen, B. Su, Efficient etching of oxygen-incorporated molybdenum disulfide nanosheet arrays for excellent electrocatalytic hydrogen evolution. Appl. Surf. Sci. **491**, 245–255 (2019). https://doi.org/10.1016/j.apsusc.2019.06.153
19. J. Xie, J. Zhang, S. Li, F. Grote, X. Zhang, H. Zhang, R. Wang, Y. Lei, B. Pan, Y. Xie, Controllable disorder engineering in oxygen-incorporated MoS_2 ultrathin nanosheets for efficient hydrogen evolution. J. Am. Chem. Soc. **135**, 17881–17888 (2013). https://doi.org/10.1021/ja408329q
20. X.-Y. Li, S.-J. Zhu, Y.-L. Wang, T. Lian, X. Yang, C.-F. Ye, Y. Li, B.-L. Su, L.-H. Chen, Synergistic regulation of S-vacancy of MoS_2-based materials for highly efficient electrocatalytic hydrogen evolution. Front. Chem. **10**, 1–17 (2022). https://doi.org/10.3389/fchem.2022.915468
21. T. Lian, X. Li, Y. Wang, S. Zhu, X. Yang, Z. Liu, C. Ye, J. Liu, Y. Li, B. Su, L. Chen, Boosting highly active exposed Mo atoms by fine-tuning S-vacancies of MoS_2-based materials for efficient hydrogen evolution. ACS Appl. Mater. Interfaces **14**, 30746–30759 (2022). https://doi.org/10.1021/acsami.2c05444
22. X. Wang, Y.Y. Zhang, H. Si, Q. Zhang, J. Wu, L. Gao, X. Wei, Y. Sun, Q. Liao, Z. Zhang, K. Ammarah, L. Gu, Z. Kang, Y.Y. Zhang, Single-atom vacancy defect to trigger high-efficiency hydrogen evolution of MoS_2. J. Am. Chem. Soc. **142**, 4298–4308 (2020). https://doi.org/10.1021/jacs.9b12113
23. S. Park, J. Park, H. Abroshan, L. Zhang, J.K. Kim, J. Zhang, J. Guo, S. Siahrostami, X. Zheng, Enhancing catalytic activity of MoS_2 basal plane S-vacancy by co cluster addition. ACS Energy Lett. **3**, 2685–2693 (2018). https://doi.org/10.1021/acsenergylett.8b01567
24. C.C. Cheng, A.Y. Lu, C.C. Tseng, X. Yang, M.N. Hedhili, M.C. Chen, K.H. Wei, L.J. Li, Activating basal-plane catalytic activity of two-dimensional MoS_2 monolayer with remote hydrogen plasma. Nano Energy **30**, 846–852 (2016). https://doi.org/10.1016/j.nanoen.2016.09.010
25. L. Li, Z. Qin, L. Ries, S. Hong, T. Michel, J. Yang, C. Salameh, M. Bechelany, P. Miele, D. Kaplan, D. Voiry, M. Chhowalla, D. Voiry, Role of sulfur vacancies and undercoordinated mo regions in MoS_2 nanosheets toward the evolution of hydrogen. ACS Nano **13**, 6824–6834 (2019). https://doi.org/10.1021/acsnano.9b01583

26. C. Tsai, H. Li, S. Park, J. Park, H.S. Han, J.K. Nørskov, X. Zheng, F. Abild-pedersen, Electrochemical generation of sulfur vacancies in the basal plane of MoS_2 for hydrogen evolution. Nat. Commun. **8**, 1–8 (2017). https://doi.org/10.1038/ncomms15113
27. P. Zhang, H. Xiang, L. Tao, H. Dong, Y. Zhou, T.S. Hu, X. Chen, S. Liu, S. Wang, S. Garaj, Chemically activated MoS_2 for efficient hydrogen poduction. Nano Energy **57**, 535–541 (2019). https://doi.org/10.1016/j.nanoen.2018.12.045
28. M. Wu, J. Liao, L. Yu, R. Lv, P. Li, W. Sun, R. Tan, X. Duan, L. Zhang, F. Li, J. Kim, K.H. Shin, H. Seok Park, W. Zhang, Z. Guo, H. Wang, Y. Tang, G. Gorgolis, C. Galiotis, J. Ma, Roadmap on carbon materials for energy storage and conversion. Chem. Asian J. **15**(2020), 995–1013 (2020). https://doi.org/10.1002/asia.201901802
29. X. Chen, B. Put, A. Sagara, K. Gandrud, M. Murata, J.A. Steele, H. Yabe, T. Hantschel, M. Roeffaers, M. Tomiyama, H. Arase, Y. Kaneko, M. Shimada, M. Mees, P.M. Vereecken, Silica gel solid nanocomposite electrolytes with interfacial conductivity promotion exceeding the bulk li-ion conductivity of the ionic liquid electrolyte filler, Sci. Adv. **6**, (2020).https://doi.org/10.1126/sciadv.aav3400
30. J. Xu, G. Shao, X. Tang, F. Lv, H. Xiang, C. Jing, S. Liu, S. Dai, Y. Li, J. Luo, Z. Zhou, Frenkel-defected monolayer MoS_2 catalysts for efficient hydrogen evolution. Nat. Commun. **13**, 2193–2201 (2022). https://doi.org/10.1038/s41467-022-29929-7
31. Y. Zheng, T. Zhou, C. Zhang, J. Mao, H. Liu, Z. Guo, boosted charge transfer in SnS/SnO_2 heterostructures: toward high rate capability for sodium-ion batteries. Angew. Chem. Int. Ed. **55**, 3408–3413 (2016). https://doi.org/10.1002/anie.201510978
32. Y. Wan, Z. Zhang, X. Xu, Z. Zhang, P. Li, X. Fang, K. Zhang, K. Yuan, K. Liu, G. Ran, Y. Li, Y. Ye, L. Dai, Engineering active edge sites of fractal-shaped single-layer MoS_2 catalysts for high-efficiency hydrogen evolution. Nano Energy **51**, 786–792 (2018). https://doi.org/10.1016/j.nanoen.2018.02.027
33. J. Lin, S. Zuluaga, P. Yu, Z. Liu, S.T. Pantelides, K. Suenaga, Novel Pd_2Se_3 two-dimensional phase driven by interlayer fusion in layered $PdSe_2$. Phys. Rev. Lett. **119**, 1700–1701 (2017). https://doi.org/10.1103/PhysRevLett.119.016101
34. Y. Dong, B. Zeng, J. Xiao, X. Zhang, D. Li, M. Li, J. He, M. Long, Effect of sulphur vacancy and interlayer interaction on the electronic structure and spin splitting of bilayer MoS_2. J. Phys. Condens. Matter **30**, 125302 (2018). https://doi.org/10.1088/1361-648X/aaad3b
35. X. Zhang, S. Wang, C.-K. Lee, C.-M. Cheng, J.-C. Lan, X. Li, J. Qiao, X. Tao, Unravelling the effect of sulfur vacancies on the electronic structure of the MoS_2 crystal. Phys. Chem. Chem. Phys. **22**, 21776–21783 (2020). https://doi.org/10.1039/C9CP07004D